# The relationship between silicon isotope fractionation in sponges and silicic acid concentration: modern and core-top studies of biogenic opal

Katharine R. Hendry[1,2] & Laura F. Robinson[1,3]

*1 Department of Marine Chemistry and Geochemistry, Woods Hole Oceanographic Institution, Woods Hole, MA 02543, USA*

*2 School of Ocean and Earth Sciences, University of Cardiff, Main Building Park Place, CF10 3AT, UK*

*3 Department of Earth Sciences, University of Bristol, Wills Memorial Building, Queen's Road, BS8 1RJ, UK*

## ABSTRACT

Recent work has shown the silicon isotope composition, denoted by $\delta^{30}Si$, of deep-sea sponges reflects the concentration of ambient silicic acid ($Si(OH)_4$) in seawater. However, existing calibrations are based predominantly on living sponges collected from the Southern Ocean. These data cannot, however, be used to determine whether other parameters that correlate with silicic acid in the Southern Ocean, such as temperature and salinity, influence $\delta^{30}Si$ of sponges. Furthermore, the published data do not demonstrate whether disaggregated core-top sedimentary spicules preserve the primary $\delta^{30}Si$ signal recorded in living sponges. Here, we address both of these issues. We refine and widen the existing calibration by including a global distribution of modern sponges. In addition, we provide the first systematic calibration from spicules picked from core-top sediments that covers sites from different ocean basins.

The relationship between $Si(OH)_4$ and $\delta^{30}Si$ in sponge spicules is the same in different ocean basins, between specimens that grew in different temperature and salinity conditions. Our core-top data agree well with the modern sponge calibration indicating there are no significant post-depositional effects or early diagenetic overprints. These two new datasets support the assertion that sponge $\delta^{30}Si$ can be used as a proxy for silicic acid concentrations in the past.

## 1. INTRODUCTION

The marine Si cycle is linked to global climate through coupling with the carbon cycle and the influence of tectonics and silicate weathering (West et al., 2005). In the modern ocean, biological precipitation of amorphous silica (opal) by diatoms is the dominant process that removes dissolved Si (silicic acid, or $Si(OH)_4$) from seawater, and is an efficient conveyor of organic carbon to the seafloor (Falkowski et al., 2004). The efficient uptake of Si by diatoms leads to a depletion of $Si(OH)_4$ in surface waters, such that in modern oceans diatom blooms are reliant on upwelling sources of $Si(OH)_4$. The nutrient composition of upwelling waters, in particular the ratio of Si to other major nutrients, plays a strong role in the population structure of phytoplankton growing in surface waters (Sarmiento et al., 2004). Quantifying changes in the nutrient composition of deep and intermediate water is necessary in order to understand changes in surface production of biogenic opal, which provides a key control on atmospheric carbon dioxide ($pCO_2$) and global climate (Brzezinski et al., 2002; de la Rocha & Bickle, 2005; Hendry et al., 2010a, Ellwood et al., 2010).

The silicon isotope composition of biogenic opal ($\delta^{29}Si$ and $\delta^{30}Si$) has already been used to study modern Si cycling and past nutrient supply and utilization. Silicon is present in three stable isotopes: $^{28}Si$ (92.22%), $^{29}Si$ (4.68%) and $^{30}Si$ (3.08%). The per mil Si isotopic composition is expressed relative to the NIST standard, NBS 28, according to Equation 1, were x is 29 or 30 (isotope ratios will be reported here as $\delta^{30}Si$):

$$\delta^{x}Si = \left\{ \frac{\left( \frac{^{x}Si}{^{28}Si} \right)_{sample}}{\left( \frac{^{x}Si}{^{28}Si} \right)_{NBS\,28}} - 1 \right\} \times 1000 \qquad (1)$$

The $\delta^{30}Si$ of biogenic opal is influenced by a number of factors including seawater $Si(OH)_4$ and biological fractionation. On timescales shorter than the residence time of Si in the ocean (estimated as between 9 and 15 thousand years; Tréguer et al., 1995; Georg et al., 2009), the isotopic composition of dissolved Si ($\delta^{30}Si(OH)_4$) in the whole ocean is unlikely to change, although there are regional and vertical differences controlled by biological productivity and ocean circulation. The $\delta^{30}Si$ of diatom opal extracted from sediment cores have been used to reconstruct changes in ocean productivity, because of the Rayleigh-type fractionation processes that occur during uptake of $Si(OH)_4$ in surface waters (de la Rocha et al., 1997, 1998). However, the interpretation of diatom $\delta^{30}Si$ is challenging because the lack of constraints on the spatial variation in $\delta^{30}Si(OH)_4$, the composition of upwelling waters, mixing and export rates (e.g. Cardinal et al., 2007).

64 Sponges are benthic filter-feeding organisms that utilize dissolved Si for skeletal
65 growth by precipitating opaline spicules of various morphologies. Recent work has
66 shown that $\delta^{30}Si$ composition of deep-sea sponges from the Southern Ocean reflects
67 the availability of dissolved Si during growth, and is therefore a potential proxy for
68 past deep and intermediate water $Si(OH)_4$ concentrations (Hendry et al, 2010a, 2011;
69 Wille et al., 2010). There are no apparent species specific effects on Si fractionation,
70 and tests on different types of spicules show that Si isotopes are homogeneous within
71 an individual (Hendry et al., 2010a). Sponge spicules are ubiquitous in sediments
72 throughout the oceans, but to date there has not been a thorough global calibration of
73 the proxy that includes other ocean basins. The inclusion of other ocean basins in
74 assessing the extent to which sponge spicules reflect $Si(OH)_4$ is important because the
75 $Si(OH)_4$ concentration in Southern Ocean waters is strongly correlated with other
76 environmental parameters such as temperature and salinity making it difficult to test
77 the influence of a single parameter. There are some differences in temperature-
78 salinity-Si regimes in the Southern Ocean, for example from coastal regions off the
79 West Antarctic Peninsula (Hendry et al., 2010a), which indicate that $Si(OH)_4$
80 concentration is indeed the major controller. However, the robustness of the $Si(OH)_4$-
81 $\delta^{30}Si$ relationship needs to be tested further by investigating modern specimens from
82 other oceanic basins and different water masses.

83 An important test of any paleoclimate proxy is whether core-top skeletal elements
84 retain the signature of modern, living specimens despite post-depositional processes
85 such as diagenesis, dissolution and averaging of vital effects over a number of
86 individuals. These types of problems have been tested in, for example, Mg/Ca of

87 planktonic foraminifera, thought to be a measure of near surface temperatures
88 (reviewed by Elderfield & Ganssen, 2000). Several studies have revealed several other
89 factors that can control foraminiferal Mg/Ca during life, including growth rate,
90 ontogeny, salinity, seasonality and vertical migration in the water column (e.g.
91 Elderfield et al., 2002; Ferguson et al., 2008, Wit et al., 2010), and during post-
92 depositional processes (e.g. Brown & Elderfield, 1996; Barker et al., 2003). As a result,
93 individual specimens from core-top sediments exhibit large variability between and
94 within individuals, and analyses show a reduction in variability as sample size
95 increases (Anand et al., 2005).

96 In contrast to foraminiferal proxies, there has been no core-top calibration of sponge
97 spicule $\delta^{30}Si$, although core-top spicules would provide a more appropriate
98 comparison for downcore records and indicate any post-mortem, post-depositional,
99 diagenetic or dissolution effects on sponge silicon isotopes. The high surface reactivity
100 of biogenic opal (Dixit & van Capellan, 2002) makes it susceptible to rapid early
101 diagenesis at the sediment-water interface. For example, the normalized aluminum
102 content of opal $(Al/Si)_{opal}$, increases over an order of magnitude between water
103 column or sediment trap samples and surficial sediments (van Beusekom et al., 1997;
104 Hendry et al., 2010b). A previous study has also found a potential diagenetic signal in
105 diatom opal $\delta^{30}Si$, thought to be a result of surface dissolution effects, which may
106 impact glacial-interglacial records by 10-30% (Demarest et al., 2009), although this is
107 unlikely to have such an impact on spicules due to their more refractory nature
108 (Maldonado et al., 2005).

Here, we extend the calibration for living specimens, and present new core-top spicule data, from the Atlantic and Pacific Oceans. We also use our data in combination with recently published experimentally derived assessments of silicon uptake rates (Maldonado et al., 2011) to explore the fractionation processes involved in biosilicification in sponges.

## 2. METHODS AND MATERIALS

### 2.1. Samples and sample preparation

Modern sponges were collected by trawl or dredge from the following localities (Table 1; Fig. 1), which have either co-located seawater samples or are located in well-constrained water masses:

- Scotia Sea and Drake Passage aboard the *R/V Nathaniel B. Palmer* in 2008 (full details in Hendry et al., 2010a);
- North Atlantic, from near Iceland, aboard the *Celtic Explorer* in 2008;
- North Pacific, from near Hawaii, *R/V Ka`Imikai-O-Kanalo*, in 2009. Further North Pacific samples were obtained from the Smithsonian collection (preserved in alcohol).

Specimens were also collected by hand by divers from the West Antarctic Peninsula and off Woods Hole, eastern Massachusetts (spring 2010).

The sponges were dried or frozen for transportation (with the exception of the samples from the Smithsonian). Organic matter was removed by heating three times in $H_2O_2$ (30% reagent grade) and then three times in concentrated in-house Teflon-

distilled $HNO_3$, followed by thorough rinsing in 18 MΩ Milli-Q water. Any remaining lithogenic particles were removed by hand, before a final clean in 50% in-house Teflon-distilled $HNO_3$/10% HCl, followed by five further Milli-Q water rinses. The spicules were dried, and 5-20mg of each sample was fused with high purity NaOH pellets (Fisher Scientific) at 730°C for 10 minutes in cleaned silver crucibles, quenched in Milli-Q water, sonicated and acidified according to Georg et al., 2006. These solutions can be stored for several months without change in $\delta^{30}Si$.

Thirty to fifty core-top spicules were picked out of sediments from the Southern Ocean, the Argentine Shelf, the Iceland Basin, the Carolina Slope (North Atlantic, Keigwin, 2001) and Akademia Nauk Rise (Okhotsk Sea, North Pacific, Keigwin, 1998; Fig. 1, Table 1). The spicules were hand-picked from coarsely-sieved sediments, cleaned for clay contaminants by sonicating in ethanol (reagent grade), rinsed, heated in $H_2O_2$ (30% reagent grade) and then dried. The spicules were dissolved in 0.2 M NaOH solution at 100°C for three days, and then acidified, according to Hendry et al., 2010a. The solutions produced by this method cannot be stored on a long-term basis without a change in isotopic composition, but it does allow preparation and analysis of small samples of core top spicules (10 - 20µg Si) that cannot be prepared with the alkaline fusion method above as it would result in a solution of very low Si concentration. Spicules were picked from sediments dredged from two sites near Sars Seamount in the Drake Passage (*R/V Nathaniel B. Palmer*, cruises NBP0805 and NBP1103), prepared by alkaline fusion (Georg et al., 2006) and analyzed.

### 2.2. Analytical Procedures

*2.2.1. Standard-sample bracketing without Mg doping*

Silicon from the dissolved samples was quantitatively separated from metal contaminants using a cation exchange resin (Georg et al., 2006; Hendry et al., 2010a). The post-column samples were introduced into the Thermo Neptune Multi-Collector Inductively Coupled Plasma Mass Spectrometer (MC-ICP-MS) instrument at the Woods Hole Oceanographic Institution (WHOI) ICP-MS Facility.

Two methods were used to analyze Si isotopes: standard-sample bracketing and Mg doping. Mg doping was used because it has previously been reported as yielding higher precision and accuracy than standard-sample bracketing alone on the Neptune MC-ICP-MS (Cardinal et al., 2003). However, both methods yield accuracy and precision that are more than adequate for paleoceanographic applications.

Full operating conditions for the standard-sample bracketing method are described in Hendry et al., 2011. Mass bias and drift were accounted for by standard-sample bracketing, intensity matching samples and bracketing standards. Values of $\delta^{29}Si$ and $\delta^{30}Si$ were calculated offline using Equation 1, taking an average of the two bracketing standards for each sample, and repeat measurements were made for each sample (n=3). Data that did not meet strict quality control criteria were rejected, meeting guidelines described in Hendry et al., 2011. Repeat measurements (n = 14 runs) of sponge standard LMG08 show long-term reproducibility (using the mean of 3 standard-sample brackets per run) over 24 months of ~ 0.06‰ for $\delta^{29}Si$ and ~0.15‰ for $\delta^{30}Si$ ($2\sigma_{SD}$, Table 1; Hendry et al., 2010a, 2011). The relationship between $\delta^{29}Si$ and $\delta^{30}Si$ for all the modern sponge material analyzed by the method (slope = 0.515 ±

0.014, intercept = 0.009 ± 0.044; model II regression, 2σ confidence interval, n = 17) is consistent with mass dependent fractionation (Reynolds et al., 2007).

*2.2.1. Standard-sample bracketing with Mg doping*

Si and Mg isotopes were measured on the Neptune MC-ICP-MS in dual mode (peak-hopping) using a method adapted from Cardinal et al. (2003), such that $^{28}Si$, $^{29}Si$ and $^{30}Si$ were measured in the first cycle and $^{24}Mg$, $^{25}Mg$ and $^{26}Mg$ measured on the second cycle, with each cycle comprising 30 alternate measurements. Typical internal precision for the Si isotope ratios is comparable to the previous standard-sample bracketing method as described above (standard deviation ~5 x $10^{-6}$). The Si blanks of the Mg solution were the same as for 5% HCl and were less than 1% of the signal on the Si peak for each sample and standard. Blanks on $^{24}Mg$ are less than 5mV (<0.05% of the signal). Samples and bracketing standards were spiked with Mg standard (Inorganic Ventures), and intensity matched for $^{28}Si$ and $^{24}Mg$ signals within 10% (typically within 5%).

Si isotope ratios were corrected according to Cardinal et al. (2003). Our measurements of $^{25}Mg/^{24}Mg$ and $^{26}Mg/^{24}Mg$ show a consistent relationship for each run, with $\ln(^{25}Mg/^{24}Mg)$ versus $\ln(^{26}Mg/^{24}Mg)$ for repeat measurements of the sponge standard LMG08 showing a slope of 0.519 ± 0.006 (model II regression, 2σ confidence interval, n = 13) over a two month period (October to November 2010), which is in agreement with previous empirical estimates of fractionation (Galy et al., 2001; Cardinal et al., 2003) and consistent with the theoretical slope for either thermodynamic (0.521) or

196 kinetic (0.511) mass-dependent fractionation (Galy et al., 2001; Young et al., 2002).
197 Within each run, ln($^{25}$Mg/$^{24}$Mg) values are linearly related to ln($^{29}$Si/$^{28}$Si). Repeat
198 measurements (n = 14 runs) of standard LMG08 (using the mean of 3 standard-sample
199 brackets per run) agree within error with previous measurements made using a range
200 of methods (Hendry et al., 2011) and shows a reproducibility of ±0.04‰ for $\delta^{29}$Si and
201 ±0.09‰ for $\delta^{30}$Si (2σ) over approximately 12 months, which is an improvement on
202 conventional standard-sample bracketing (0.05‰ for $\delta^{29}$Si and 0.15‰ for $\delta^{30}$Si, 2σ).
203 Repeat measurements of sample aliquots, within and between runs, show typical
204 variability <±0.1‰ for $\delta^{29}$Si and $\delta^{30}$Si.

205 **3. RESULTS AND DISCUSSION**

206 The aim of this study was to investigate the possible link between seawater $Si(OH)_4$
207 concentrations and the isotopic composition of living sponges and core-top spicules
208 by comparing data collected from specimens from other ocean basins to previously
209 studied Southern Ocean samples. Here, we will discuss the modern and core-top
210 spicule results, and present a biosilicification model that investigates the fractionation
211 of isotopes by sponges during $Si(OH)_4$ uptake.

212 *3.1. Sponge $\delta^{30}$Si from living specimens*

213 The modern sponge $\delta^{29}$Si values range from +0.21‰ to -2.99‰ and $\delta^{30}$Si range from
214 +0.48‰ to -5.72‰ (Fig. 2A, Table 1). The core-top values fall within a similar range of
215 $\delta^{30}$Si values, from -0.93‰ to -3.86‰ (Table 1).

Quantifying the fractionation of Si isotopes during the precipitation of biogenic opal requires values for the isotopic composition of both the opal and dissolved silicon in seawater in which the sponge grew ($\delta^{30}Si(OH)_4$; Table 2). Si isotope fractionation by the sponges can be approximated to the difference between the isotopic composition of the seawater (Table 2) and the spicules assuming the opal is in equilibrium with the surrounding medium, which we will refer to as the "apparent isotope fractionation":

$$\varepsilon_{Si} \approx \Delta\delta^{30}Si = \delta^{30}Si_{opal} - \delta^{30}Si_{seawater} \quad (2)$$

Deep-sea sponges live in a stable physical and chemical environment making it reasonable to assume that they show apparent isotopic fractionation in equilibrium with the surrounding medium. However, seawater $\delta^{30}Si(OH)_4$ values are relatively poorly constrained due to limited datasets and natural variability, so a degree of uncertainty must be placed on calculated values of $\Delta\delta^{30}Si$ (~0.4-0.5‰; see Fig. 2B).

$\Delta\delta^{30}Si$ in the low $Si(OH)_4$ North Atlantic sponges ranged between approximately -1‰ and -2‰, The sponge from the coastal region (very low $Si(OH)_4$) near Woods Hole showed the heaviest isotopic compositions. The $\Delta\delta^{30}Si$ in $Si(OH)_4$–enriched North Pacific sponges was greater, ranging between approximately -5‰ and -6‰, with one as isotopically light as -6.5‰ (Fig. 2B). This result is in agreement with previous findings that the apparent Si isotopic fractionation in sponges is related to ambient $Si(OH)_4$ concentration (Fig. 2B; Hendry et al., 2010a; Wille et al., 2010; Hendry et al., 2011). A non-linear regression, fitting the dataset to a hyperbolic decay function, shows that the relationship between isotopic fractionation by sponges and ambient $Si(OH)_4$ is statistically significant ($R^2$=0.85 for $\delta^{30}Si$ and $R^2$=0.83 for $\Delta\delta^{30}Si$; n = 62).

238 It is difficult to determine what factors control Si isotope fractionation in sponges from
239 the Southern Ocean because there is such a strong correlation between environmental
240 parameters such as $Si(OH)_4$ concentration, temperature and salinity. However, we can
241 use the new data from other ocean basins and water masses with different
242 temperature and salinity properties to deconvolve the influence of different
243 environmental parameters and $\delta^{30}Si$. In contrast to the Southern Ocean plot, the plot
244 of sponge $\Delta\delta^{30}Si$ versus temperature for samples from the North Atlantic and North
245 Pacific shows that there is, in fact, no apparent influence of temperature (Fig. 3).
246 Silicification in sponges is controlled by enzymatic processes, which would suggest
247 that temperature could play an important role in Si uptake rates. However,
248 experiments with live sponges show that increasing temperature does not influence Si
249 uptake rates, consistent with our findings if Si uptake rate is the primary control over
250 Si isotope fractionation (Frølich & Barthel, 1997). In addition to temperature, the data
251 also show that there is no likely control on fractionation by salinity. The sponges
252 grown in the North Pacific, for example, under similar $Si(OH)_4$ conditions have similar
253 $\Delta\delta^{30}Si$ to those grown in the Southern Ocean despite having grown in significantly
254 fresher waters (34.25-34.5 vs. ~34.7 in the Southern Ocean, all data from
255 www.ewoce.org).

256 One important consideration of the results and interpretation of our data set in terms
257 of major controls on silicification is that the sponge $\delta^{30}Si$ dataset presented here is
258 dominated by samples from the deep-ocean (with the exception of two surface water
259 sponges) and so not cover the entire range of environmental conditions of sponge

habitats. Further studies of shallow-living sponges, and particularly specimens from tropical shallow seas, would be helpful in extending our understanding of the differences and similarities of biosilificiaotin in different habitats. However, our study does show that for the sub-thermocline conditions relevant to paleoceanographic applications based on spicules extracted from deep-sea sediment cores, the ambient $Si(OH)_4$ concentration is the dominant control over spicule $\delta^{30}Si$, supporting the use of sponge $\delta^{30}Si$ as a robust paleosilicic acid proxy.

### *3.2. Silicon fractionation model*

Silicon uptake kinetics in sponges have been investigated through culture experiments on living specimens grown in media of differing $Si(OH)_4$ concentrations. Two different experimental set-ups have been used: initially based on explants, or pieces of sponges that have regenerated (Reincke & Barthel, 1997), and more recently on whole sponge specimens (Maldonado et al., 2011). In both cases, dissolved silicon was added to the growth medium in varying amounts, in the form of either $Na_2SiF_6$, which can result in fluoride poisoning at high Si concentrations (>200 μM Si), or $Na_2SiO_3.5H_2O$. The $Si(OH)_4$ concentrations in the growth medium are measured periodically to determine the Si uptake rate and at the end of the experiments the volume, wet and dry weights of the sponges are determined. Despite the differences in experimental set-up, both experiments show a non-linear relationship between silicon uptake and silicic acid concentration, resembling a Michaelis-Menton function (Reincke & Barthel, 1997; Maldonado et al., 2011).

281 The nature of the relationship between $Si(OH)_4$ concentration and uptake rate in
282 sponges resembles that between $Si(OH)_4$ and Si isotopic fractionation. This non-linear
283 relationship between $\Delta\delta^{30}Si$ and $Si(OH)_4$ is likely a result of fractionation during Si
284 uptake, whereby as Si uptake rates increase with concentration, fractionation involved
285 with these uptake processes also becomes enhanced (Wille et al., 2010). Although
286 there are likely to be additional factors, this effect can be modeled assuming that the
287 fractionation occurs in several steps: firstly as the Si is transported into the cell,
288 secondly as the Si is polymerized, and thirdly as Si is lost from the cell (Fig. 4A).

289 Here, we build on the method developed by Wille et al. (2010), integrating i) our new
290 data from different ocean basins, which shows that the fractionation processes appear
291 to be universal in sponges grown in markedly different environments , and ii) the
292 recent experimental Si uptake data from Maldonado et al. (2011).

293 The fractionation process can be expressed mathematically following Milligan et al.,
294 2004 (Equation 3):

295 $$\Delta\delta^{30}Si \approx \varepsilon_f = \varepsilon_{tI} + (\varepsilon_p - \varepsilon_{tE})\frac{\nu_E}{\nu_I} \quad (3)$$

296 Where $\varepsilon_f$ = the total Si isotopic fractionation factor, $\varepsilon_{tI}$ = Si isotopic fractionation
297 associated with transport into the cell, $\varepsilon_p$ = Si isotopic fractionation associated with
298 polymerization and $\varepsilon_{tE}$ = Si isotopic fractionation associated with transport out of the
299 cell; $\nu_E$ = rate of Si efflux and $\nu_I$ = rate of Si influx (Fig. 4A). This equation has been
300 rearranged by Wille et al. (2010) to form Equations 4 and 5:
301

$$\varepsilon_f = \varepsilon_{tI} + \Delta\varepsilon_p \left\{ 1 - \frac{\dfrac{\nu_{\max p}}{\left(\dfrac{K_{mp}}{[Si(OH)_4]}\right)+1}}{\dfrac{\nu_{\max I}}{\left(\dfrac{K_{mI}}{[Si(OH)_4]}\right)+1}} \right\} \quad (4)$$

$$K_{mI} = \nu_{\max I} \times \frac{K_{mp}}{\nu_{\max p}} \quad (5)$$

where $\Delta\varepsilon_p = (\varepsilon_p - \varepsilon_{tE})$; $K_{mI}$ and $K_{mp}$ are the half saturation constants for incorporation and polymerization respectively, and $\nu_{maxI}$ and $\nu_{maxp}$ are the maximum incorporation and polymerization rates respectively. $K_m$ is defined as the concentration at which the reaction rate is half of its maximum value ($\nu_{max}$). In this case a low value of $K_m$ represents a high affinity for $Si(OH)_4$.

$K_{mp}$ and $\nu_{maxp}$ are poorly constrained, and highly variable even within a species (e.g. Maldonado et al., 2011). The two uptake experiments to date yielded $K_{mp}$ and $\nu_{maxp}$ values of 46 μM and 19 μmol $h^{-1}$ $g^{-1}$ (*Halichondria panicea*; Reincke & Barthel, 1997), and 74 μM and 1.7 μmol $h^{-1}$ $g^{-1}$ (ranging from 0.03 to 5.2 μmol $h^{-1}$ $g^{-1}$ for dry weights) respectively (*Axinella* spp; Maldonado et al., 2011). For every $\nu_{maxI}$ there is a unique value of $\Delta\varepsilon_p$ that corresponds to the minimum of the misfit function for a given dataset (Equation 6).

$$f(\varepsilon_{tI}, \Delta\varepsilon, \nu_{\max I}) = \sum_{[Si(OH)_4]} (\varepsilon_{f,obs}([Si(OH)_4]) - \varepsilon_{f,pred}([Si(OH)_4]))^2 \quad (6)$$

Wille et al. (2010) found that, using the values for $K_m$ and $\nu_{maxp}$ from Reincke & Barthel (1997), varying $\nu_{maxI}$ has little impact on the value of $\Delta\varepsilon_p$ at which the misfit function is at a minimum for values greater than ~ 40 μmol $h^{-1}$ $g^{-1}$ so in this model we used a fixed

$\nu_{maxI}$ of 120 μmol $h^{-1}$ $g^{-1}$. We varied the remaining constants ($\varepsilon_{tI}$ and $\Delta\varepsilon_p$) to predict $\Delta\delta^{30}Si$ using Equations 4 and 5, and optimized by finding the minimum of the misfit between predicted and measured $\Delta\delta^{30}Si$ (Equation 7):

$$f(\varepsilon_{tI}, \Delta\varepsilon) = \sum_{[Si(OH)_4]} (\varepsilon_{f,obs}([Si(OH)_4]) - \varepsilon_{f,pred}([Si(OH)_4]))^2 \quad (7)$$

Using only the values of $K_{mp}$ and $\nu_{maxp}$ from Reincke & Barthel (1997) yields $\varepsilon_{tI}$ = -1.55‰ and $\Delta\varepsilon_p$ = -5.3‰ for the whole dataset, and $\varepsilon_{tI}$ = -1.46 and $\Delta\varepsilon_p$ = -5.4‰ for the Southern Ocean sponges considered alone (Fig. 4B). These are both slightly greater influx fractionations than that found by Wille et al. (2010) of -1.34‰, but all three values are within the uncertainties associated with the data.

Substituting the values of $\nu_{maxp}$ and $K_{mp}$ that Maldonado et al. (2011) determined yields minimum misfit values of $\varepsilon_{tI}$ and $\Delta\varepsilon_p$ of -1.74‰ and -5.11‰ for all modern sponges, a level of influx fractionation that is greater than the uncertainty in the data (Fig. 4C). The differences between the two datasets could have arisen due to bias in the two contrasting experimental set-ups, for example as a result of the physiological differences between explants, which show rapid regenerative growth, and whole specimens, or due to adverse effects of the dissolved silicon added to the medium (Maldonado et al., 2011). However, perhaps more importantly, the two studies focus on two different types of sponge. *H. panacea* is a seasonal sponge, silicifying rapidly in the spring for only a couple of months. In contrast, *Axinella* spp. Is a slow growing, long-lived sponge that can lives for decades (Maldonado et al., 2011). Such differences in growth behavior highlights that care must be taken when extrapolating the uptake kinetics of shallow-water sponges to our predominantly deep-water sponge dataset.

345 Nonetheless, this model is a useful first approach for understanding and quantifying Si
346 isotope fractionation in sponges.

347 The fractionation constants calculated above were used to predict the sponge $\Delta\delta^{30}Si$
348 for each location in the dataset using Equations 4 and 5. As predicted from the prior
349 misfit analysis, the observed and predicted $\Delta\delta^{30}Si$ values show a significant positive
350 correlation ($r^2 = 0.82$ for both sets of uptake kinetics parameters) and the majority fall
351 within error of a 1:1 line (Fig. 5). The exceptions are the sponges grown in very high
352 $Si(OH)_4$ waters of the North Pacific (>120-130 μM). At such extreme Si availability, it
353 could be that the relationship between net uptake, polymerization and ambient
354 $Si(OH)_4$ weakens. Under very high $Si(OH)_4$ availability, hypersilicification can occur
355 and is known to happen at $Si(OH)_4$ concentrations greater than 100 μM, which could
356 alter the apparent Si isotope fractionation (Maldonado et al., 1999). There is further
357 evidence for a fundamental change in the fractionation mechanism at very high
358 $Si(OH)_4$ from the core-top sample from Okhotsk Sea ($Si(OH)_4$ ~200 μM). However, the
359 hypersilicification studies were carried out in shallow-living sponges from the
360 Mediterranean and it is not yet known whether the same processes would occur in
361 deep-sea sponges. Another possibility is that there are variations in deep water
362 $\delta^{30}Si(OH)_4$ that are not captured by the values used in the model (Table 2). Further
363 work is required to constrain the behavior of Si isotopes in both seawater and biogenic
364 opal at extreme $Si(OH)_4$ concentrations.

365 It should be noted that the model used in our discussion is a simplification of sponge
366 silicification. For example, the smaller microscleres may silicify in a different manner

367 to the large megascleres, which may complete formation external to the silicifying cell
368 (reviewed by Müller et al., 2007), and there is evidence for different silicification
369 mechanisms in demosponges compared to hexactinellids (Maldonado & Riesgom
370 2007). Understanding silicification mechanisms, and how they differ between
371 individuals and clades, will be an important component in understanding Si isotope
372 fractionation in sponges.

373 *3.2.1. A comparison of sponges and diatoms*

374 Above we have discussed the evidence for and possible mechanism behind variable
375 fractionation factors in deep-sea sponges. By contrast, culture experiments have been
376 used as evidence for a constant fractionation factor during Si uptake by diatoms,
377 independent of temperature and species (de la Rocha et al., 1997). However, given
378 that there is a relationship between silicic acid and growth rate in diatoms (e.g.
379 Paasche, 1973; Nelson et al., 2001), and assuming fractionation processes occur during
380 Si influx, polymerization and efflux, one might expect a link between Si isotope
381 fractionation and ambient $Si(OH)_4$ concentration. One possible test of this
382 fractionation is to investigate diatom Si uptake in natural settings. However, although
383 reasonable for deep-sea sponges, the assumption of apparent equilibrium
384 fractionation may not be necessarily be valid for diatoms because they can deplete
385 ambient $Si(OH)_4$ during growth, and because surface waters are susceptible to
386 processes such as upwelling, and advection or mixing of water masses.

387 In an attempt to account for this potential bias, we have collated data from the
388 literature that are most likely to have grown in seawater of known composition. These

389 data include plankton tow samples with water collected concurrently, and sea-ice
390 diatom samples filtered directly from melted pack ice (Varela et al., 2004; Cardinal et
391 al., 2005; Fripiat et al., 2009; Fig. 6). We also include a core-top sample from a
392 nutrient-rich region of coastal Antarctica (Table 1), where the seasonal uptake of
393 $Si(OH)_4$ is relatively low such that the water is unlikely to experience large variations
394 in $\delta^{30}Si(OH)_4$. The apparent fractionation is also known from culture experiments, and
395 varies between -0.4 to -1.6‰, with an average value of -1.1‰ (de la Rocha et al.,
396 1997). The compiled data suggest that diatoms carry out statistically significant
397 greater apparent fractionation in higher $Si(OH)_4$ concentrations ($R^2$ = 0.49, n = 27).
398 This apparent increase in fractionation factor with $Si(OH)_4$ concentration could be a
399 result of uncertainty in the relationship between the water samples and the diatom
400 samples (e.g. Cardinal et al., 2005). This finding would be consistent with culture
401 experiments that appear to show that the fractionation factor in diatoms is
402 approximately constant (de la Rocha et al., 1997). However, it is also possible that the
403 link between $Si(OH)_4$ concentration and Si isotope fractionation by sponges is a real
404 biological phenomenon and further investigation is required to prove or disprove such
405 a relationship.

406 *3.3. Core-top spicules*

407 The core-top $\delta^{30}Si$ data for sponges, for samples located near seawater silicon isotope
408 measurements or from well-characterized water masses, agree well with the
409 calibration for living specimens (Fig. 2A, B). As with other studies of this nature, it is
410 challenging to find co-located samples with a global distribution of the ideal range of

411 silicic acid concentrations. In this study, we have combined targeted collections with
412 existing cores selected to be near existing water silicon isotope analyses.
413 The one exception is the Si isotope composition of the Okhotsk Sea, which is not yet
414 known, so the value used here is from the North East Pacific as reported in Beucher et
415 al. (2008).

416 The agreement between core-top spicules and modern sponges indicate there is no
417 significant influence of early post-depositional dissolution or diagenesis on sponge
418 $\delta^{30}Si$. Laboratory studies carried out by Demarest et al (2009) on diatom cultures
419 show that the impact of dissolution on diatom opal $\delta^{30}Si$ is measurable but unlikely to
420 be significant in sediments, suggesting sponge and diatom opal may behave in a
421 similar way in a post-depositional setting.

422 The core-top calibration shows less scatter than values based on measurements of
423 individual modern sponges. This could be in part a consequence of the fact that there
424 are fewer core-top measurements and in part that some of the core-top values were
425 measured using Mg doping, whereas all of the modern sponges were measured by
426 conventional standard-sample bracketing. However, the improvement in uncertainty
427 afforded by Mg doping is less than the scatter in the modern calibration data and
428 cannot explain all of the variability observed. This result suggests that there is some
429 natural variability between individuals, possibly due to small-scale variation in
430 $Si(OH)_4$ concentration or variable physiological conditions, which is averaged out
431 through the mixing of spicules from different individuals during early sedimentation.

Although the relationship between $\delta^{30}Si$ and $Si(OH)_4$ is non-linear (Fig. 2A), the proxy works well in a range (between 5-120 μM) suitable for the majority of Quaternary paleoceangraphic applications. Taking the data within this range, it is possible to simplify the fractionation model described above by assuming a linear relationship between 5-120 μM, or by assuming a hyperbolic relationship between $Si(OH)_4$ and $\delta^{30}Si$ ($R^2$ = 0.95, n=8, for samples <120 μM; $R^2$ = 0.95, n=9, for all samples) or $\Delta\delta^{30}Si$ ($R^2$ = 0.99, n=8, for samples <120 μM; $R^2$ = 0.92, n=9, for all samples). The function that best fits the relationship between $Si(OH)_4$ and $\Delta\delta^{30}Si$ is given by Equation 8 (numbers in parentheses show $1\sigma_{SD}$):

$$\Delta\delta^{30}Si = -6.54\ (0.60) + 270(20)/\{53(20) + Si(OH)_4\ ^{*}\} \quad (8)$$

Statistical analyses indicate that this fit can predict $Si(OH)_4$ within ± 15 μM, which is an improvement on previously reported uncertainty based on individual sponges (Fig. 7). Although it would be beneficial to obtain more data from other core-top locations to test the proxy further, our results from modern and core-top samples demonstrate that the $\delta^{30}Si$ value of sponge spicules from sediments can be used to reconstruct past $Si(OH)_4$ concentrations in the ocean, and these analyses are well suited to addressing paleoceanographic questions relating to the cycling and transport of silica. Given the analytical uncertainties involved and the residence time of Si in the ocean, the relevant timescale and problems that can be addressed are on the order of ~10 ka, over which whole ocean changes in $\delta^{30}Si$ are unlikely to impact biogenic opal isotopic compositions (Georg et al., 2009). For example, one of the key applications of the

* Note: $\Delta\delta^{30}Si$ and $Si(OH)_4$ were mistakenly switched in published version

sponge $\delta^{30}Si$ proxy, tracing the movement of major water masses over glacial-interglacial timescales, requires only the distinction between high $Si(OH)_4$ (>100 μM) and low $Si(OH)_4$ (<30 μM) concentrations.

## 4. SUMMARY

In this study, we presented a calibration of modern individual sponge specimens and core-top spicules from different ocean basins. We show the relationship between sponge $\delta^{30}Si$ and $Si(OH)_4$ is the same between different ocean basins and water masses with different temperature and salinity profiles. This result provides robust evidence that $Si(OH)_4$ is indeed the major controlling factor in determining apparent sponge Si fractionation. The relationship between $\delta^{30}Si$ and $Si(OH)_4$ is consistent with a fractionation model, where Si isotopes are fractionated by sponges during uptake, polymerization and efflux. We also show that core-top $\delta^{30}Si$ values agree well with the $Si(OH)_4$ calibration of living sponges, indicating there are no significant post-depositional, dissolution or early diagenetic overprints, which have been found to impact other biogenic opal geochemical proxies.

Acknowledgements:

The authors would like to thank the following for collection of sponge specimens: Dann Blackwood (USGS, Woods Hole), Rhian Waller (University of Maine), Chris Kelley (University of Hawaii), Nicholas White (University of Cambridge), Jade Berman and Andy Clarke (British Antarctic Survey). Further specimens were obtained from the Smithsonian. Hawaiian samples were collected with Papahanaumokuakea Monument permit # PMNM-2009-053. Core samples were obtained with the assistance of Lloyd Keigwin and Ellen Roosen (WHOI), Stefan Mulitza (University of Bremen), Claire Allen and Claus-Deiter Hillenbrand (BAS), and Jerry McManus (Lamont Doherty Earth Observatory, Columbia University). Many thanks to Jurek Blusztjan and Maureen Auro (WHOI), Mark Brzezinski and Charlotte Beucher (University of California Santa Barbara), Ros Rickaby and Alex Halliday (Oxford University) for assistance in the laboratory, and with analyses and discussion. Thanks to Mark Brzezinski, Martin Wille,

James McManus and an anonymous reviewer for constructive reviews of the manuscript. Many thanks to the captain and crew of the R/V Nathaniel B Palmer (dredge samples were collected on cruises NBP0805 and NBP1103). This work was funded by the National Science Foundation (MGG grants 1029986; OPP ANT grants 0944474 and 0902957) and with the support of a WHOI Doherty Scholarship.

References:

Anand, P. and Elderfield, H., 2005. Variability of Mg/Ca and Sr/Ca between and within the planktonic foraminifers Globigerina bulloides and Globorotalia truncatulinoides. *Geochemistry Geophysics Geosystems* **6**: doi:10.1029/2004GC000811.

Barker, S., Greaves, M. et al., 2003. A study of cleaning procedures used for foraminiferal Mg/Ca paleothermometry. *Geochemistry Geophysics Geosystems* **4**, 8407.

Beucher, C. P., Brzezinski, M. A., and Jones, J. L., 2008. Sources and biological fractionation of silicon isotopes in the Eastern Equatorial Pacific. *Geochimica et Cosmochimica Acta* **72**, 3063-3073.

Brown, S. J. and Elderfield, H., 1996. Variations in Mg/Ca and Sr/Ca ratios of planktonic foraminifera caused by postdepositional dissolution: evidence of a shallow Mg-dependent dissolution. Paleoceanography 11, 543-551.

Nelson, D.K., Brzezinski, M.A., Sigman, D.E., and Franck, V.M., 2001, A seasonal progression of Si limitation in the Pacific sector of the Southern Ocean. *Deep-Sea Research II*, **48**, 3973-3995.

Brzezinski, M. A., Sigman, D. M., Sarmiento, J. L., Matsumoto, K., Gruber, N., Rau, G. H., and Coale, K. H., 2002. A switch from $Si(OH)_4$ to $NO_3^-$ depletion in the glacial

Southern Ocean. *Geophysical Research Letters* **29**, 1564.

Cardinal, D., Alleman, L. Y., de Jong, J., Ziegler, K., and Andre, L., 2003. Isotopic composition of silicon measured by multicollector plasma source mass spectrometry in dry plasma mode. *Journal of Analytical Atomic Spectrometry* **18**, 213-218.

Cardinal, D., Alleman, L. Y., Dehairs, F., Savoye, N., Trull, T. W., and Andre, L., 2005. Relevance of silicon isotopes to Si-nutrient utilization and Si-source assessment in Antarctic waters. *Global Biogeochemical Cycles* **19**, doi:10.1029/2004GB002364.

Cardinal, D., Savoye, N., Trull, T. W., Dehairs, F., E.E., K., Fripiat, F., Tison, J.-L., and André, L., 2007. Silicon isotope in spring Southern Ocean diatoms: large zonal changes despite homogeneity among size fractions. *Marine Chemistry* **106**, 46-62.

de la Rocha, C., Brzezinski, M. A., and DeNiro, M. J., 1997. Fractionation of silicon isotopes by marine diatoms during biogenic silica formation. *Geochimica Cosmochimica Acta* **61**, 5051-5056.

de la Rocha, C., Brzezinski, M. A., DeNiro, M. J., and Shemesh, A., 1998. Silicon isotope composition of diatoms as an indicator of past oceanic change. *Nature* **395**, 680-683.

de la Rocha, C. L., Brzezinski, M. A., and DeNiro, M. J., 2000. A first look at the distribution of the stable isotopes of silicon in natural waters. *Geochimica et Cosmochimica Acta* **64**, 2467-2477.

de la Rocha, C. and Bickle, M., 2005. Sensitivity of silicon isotopes to whole-ocean

changes in the silica cycle. *Marine Geology* **217**, 267-282.

Demarest, M. S., Brzezinski, M. A., and Beucher, C., 2009. Fractionation of silicon isotopes during biogenic silica dissolution. *Geochimica et Cosmochimica Acta* **73**, 5572-5583.

Dixit, S. and Van Cappellen, P., 2002. Surface chemistry and reactivity of biogenic silica. *Geochimica Cosmochimica Acta* **66**, 2559-2568.

Elderfield, H. and Ganssen, G., 2000. Past temperature and $\delta^{18}O$ of surface ocean waters inferred from foraminiferal Mg/Ca ratios. *Nature* **405**, 442-445.

Elderfield, H., Vautravers, M. et al., 2002. The relationship between shell size and Mg/Ca, Sr/Ca, d18O, and d13C of species of planktonic foraminifera. *Geochemistry Geophysics Geosystems* **3**, doi:10.1029/2001GC000194.

Ellwood, M. J., Wille, M., and Maher, W., 2010. Glacial silicic acid concentrations in the Southern Ocean. *Science* **330**, 1088-1091.

Falkowski, P. G., Katz, M. E., Knoll, A. H., Quigg, A., Raven, J. A., Schofield, O., and Taylor, F. J. R., 2004. The evolution of modern eukaryotic phytoplankton. *Science* **305**, 354-360.

Ferguson, J. E., G. M. Henderson, et al., 2008. Systematic change of foraminiferal Mg/Ca ratios across a strong salinity gradient. *Earth and Planetary Science Letters* **265**, 153-166.

Fripiat, F., Cardinal, D., Tison, J.-L., Worby, A., and André, L., 2007, Diatom-induced silicon isotopic fractionation in Antarctic sea ice. *Journal of Geophysical Research*, **112**, doi:10.1029/2006JG000244.

Frøhlich, H. and Barthel, D., 1997. Silica uptake of the marine sponge *Halichondria*

552 *panicea* in Kiel Bight. *Marine Biology* **128**, 115-125.
553 Galy, A., Belshaw, N. S., Halicz, L., and O'Nions, R. K., 2001. High-precision measurement
554 of magnesium isotopes by multiple-collector inductively coupled plasma mass
555 spectrometry. *International Journal of Mass Spectrometry* **208**, 89-98.
556 Georg, R. B., Reynolds, B. C., Frank, M., and Halliday, A. N., 2006. New sample
557 preparation techniques for the determination of Si isotopic composition using
558 MC-ICPMS. *Chemical Geology* **235**, 95-104.
559 Georg, R. B., West, A. J., Basu, A. R., and Halliday, A. N., 2009. Silicon fluxes and isotope
560 composition of direct groundwater discharge into the Bay of Bengal and the
561 effect on the global ocean silicon budget. *Earth and Planetary Science Letters*
562 **283**, 67-74.
563 Hendry, K. R., Georg, R. B., Rickaby, R. E. M., Robinson, L. F., and Halliday, A. N., 2010a.
564 Deep ocean nutrients during the Last Glacial Maximum deduced from sponge
565 silicon isotopic compositions. *Earth and Planetary Science Letters* **292**, 290-300.
566 Hendry, K. R., Meredith, M. P., Measures, C. I., Carson, D. S., and Rickaby, R. E. M., 2010b.
567 The role of sea ice formation in cycling of aluminium in northern Marguerite
568 Bay, Antarctica. *Estuarine, Coastal and Shelf Science* **87**, 103-112.
569 Hendry, K.R., Leng, M.J., Robinson, L.F., Sloane, H.J., Blusztjan, J., Rickaby, R.E.M., Georg,
570 R.B. & Halliday, A.N., 2011. Silicon isotopes in Antarctic sponges: an
571 interlaboratory comparison. *Antarctic Science* doi:
572 10.1017/S0954102010000593

573 Hendry, K.R., Robinson, L.F., Meredith, M.P., Mulitza, S., Cheissi, C., & Arz, H., in review.
574 Abrupt changes in high-latitude nutrient supply to the Atlantic during the last
575 glacial cycle.
576 Jacques, G., 1983. Some ecophysiological aspects of Antarctic phytoplankton. *Polar*
577 *Biology* **2**, 27-33.
578 Keigwin, L. D., 1998. Glacial-age hydrography of the far northwest Pacific Ocean.
579 *Paleoceanography* **13**, 323-339.
580 Keigwin, L. D., 2001. Data report: Late Pleistocene stable isotope studies of ODP sites
581 1054, 1055, and 1063. *Proceedings of the Ocean Drilling Program, Initial Reports.*
582 *College Station, Texas (Ocean Drilling Program)* **172**, 1-14.
583 Maldonado, M., Carmona, M. C., Uriz, M. J., and Cruzado, A., 1999. Decline in Mesozoic
584 reef-building sponges explained by silicon limitation. *Nature* **401**, 785-788.
585 Maldonado, M., Carmona, M.C., Velasquez, Z., Puig, A., Cruzado, A., Lopez, A., and Young,
586 C.M., 2005, Siliceous sponges as a silicon sink: an overlooked aspect of
587 benthopelagic coupling in the marine silicon cycle. *Limnology and*
588 *Oceanography*, **50**, 799-809.
589 Maldonado, M., and Riesgo, A., 2007, Intra-epitheial spicules in a homosclerophorid
590 sponge: *Cell and Tissue Research*, **328**, 639-650.
591 Maldonado, M., Navarro, L., Grasa, A., Gonzalez, A., and Vaquerizo, I., 2011. Silicon
592 uptake by sponges: a twist to understanding nutrient cycling on continental
593 margins. *Nature Scientific Reports* **1**, doi:10.1038/srep00030.
594 Milligan, A. J., Varela, D. E., Brzezinksi, M. A., and Morel, F. M. M., 2004. Dynamics of
595 silicon metabolism and silicon isotopic discrimination in a marine diatom as a

function of pCO2. Limnology and Oceanography 49, 322-329.

Müller, W.E.G., Li, J., Schroeder, H.C., Qiao, L., and Wang, X., 2007, The unique skeleton of siliceous sponges (Porifera; Hexactinellida and Demospongiae) that evolved first from the Urmetazoa during the Proterozoic: a review: *Biogeosciences*, **4**, 219-232.

Paasche, E., 1973. Silicon and the ecology of marine plankton diatoms. II. Silicate-uptake kinestics in five diatom species. *Marine Biology* **19**, 262-269.

Reincke, T. and Barthel, D., 1997. Silica uptake kinetics of Halichondria panicea in Kiel Bight. *Marine Biology* **129**, 591-593.

Reynolds, B. C., 2009. Modeling the modern marine $\delta^{30}$Si distribution. *Global Biogeochemical Cycles* **23**, GB2015, doi:10.1029/2008GB003266.

Reynolds, B. C., Aggarwal, J., Andre, L., Baxter, D., Beucher, C., Brzezinski, M. A., Engstrom, E., Georg, R. B., Land, M., Leng, M. J., Opfergelt, S., Rodushkin, I., Sloane, H. J., van der Boorn, S. H. J. M., Vroon, P. Z., and Cardinal, D., 2007. An inter-laboratory comparison of Si isotope reference materials. *Journal of Analytical Atomic Spectrometry* **22**, 561-568.

Sarmiento, J. L., Gruber, N., Brzezinski, M. A., and Dunne, J. P., 2004. High-latitude controls of thermocline nutrients and low latitude biological productivity. *Nature* **427**, 56-60.

Schröder, H. C., Wang, X. et al., 2008. Biofabrication of biosilica-glass by living organisms. *Natural Products Reports* **25**, 433-636.

Tréguer, P., Nelson, D. M., Van Bennekom, A. J., DeMaster, D. J., Leynaert, A., and Quéguiner, B., 1995. The silica balance in the world ocean: a reestimate. *Science* **268**,

375-379.

West, A. J., Galy, A., and Bickle, M., 2005. Tectonic and climatic controls on silicate weathering. *Earth and Planetary Science Letters* **235**, 211-228.

Wille, M., Sutton, J., Ellwood, M. J., Sambridge, M., Maher, W., Eggins, S., and Kelly, M., 2010. Silicon isotopic fractionation in marine sponges: a new model for understanding silicon isotopic fractionation in sponges. *Earth and Planetary Science Letters*, doi:10.1016/j.epsl.2010.01.036.

Wit, J. C., Reichart, G.-J., et al., 2010. Approaches to unravel seasonality in sea surface temperatures using paired single-specimen foraminiferal $\delta^{18}O$ and Mg/Ca analyses. *Paleoceanography* **25**, doi:10.1029/2009PA001857.

Van Beusekom, J. E. E., Bennekom, A. J., Tréguer, P., and Morvan, J., 1997. Aluminium and silicic acid in water and sediments of the Enderby and Crozet Basins. *Deep-Sea Research II* **44**, 987-1003.

Varela, D.E., Pride, C.J., and Brzezinski, M.A., 2004, Biological fractionation of silicon isotopes in Southern Ocean surface waters. *Global Biogeochemical Cycles*, **18**, doi:10.1029/2003GB002140.

Young, E. D., Galy, A., and Nagahara, H., 2002. Kinetic and equilibrium mass-dependent isotope fractionation laws in nature and their geochemical and cosmochemical significance. *Geochimica et Cosmochimica Acta* **66**, 1095-1104.

639 Figure 1: Location of samples in this study. The white circles show core-top samples,
640 the black circles show living specimens (from this study, Hendry et al., 2010a and Wille
641 et al., 2010). Drawn using GeoMapApp.

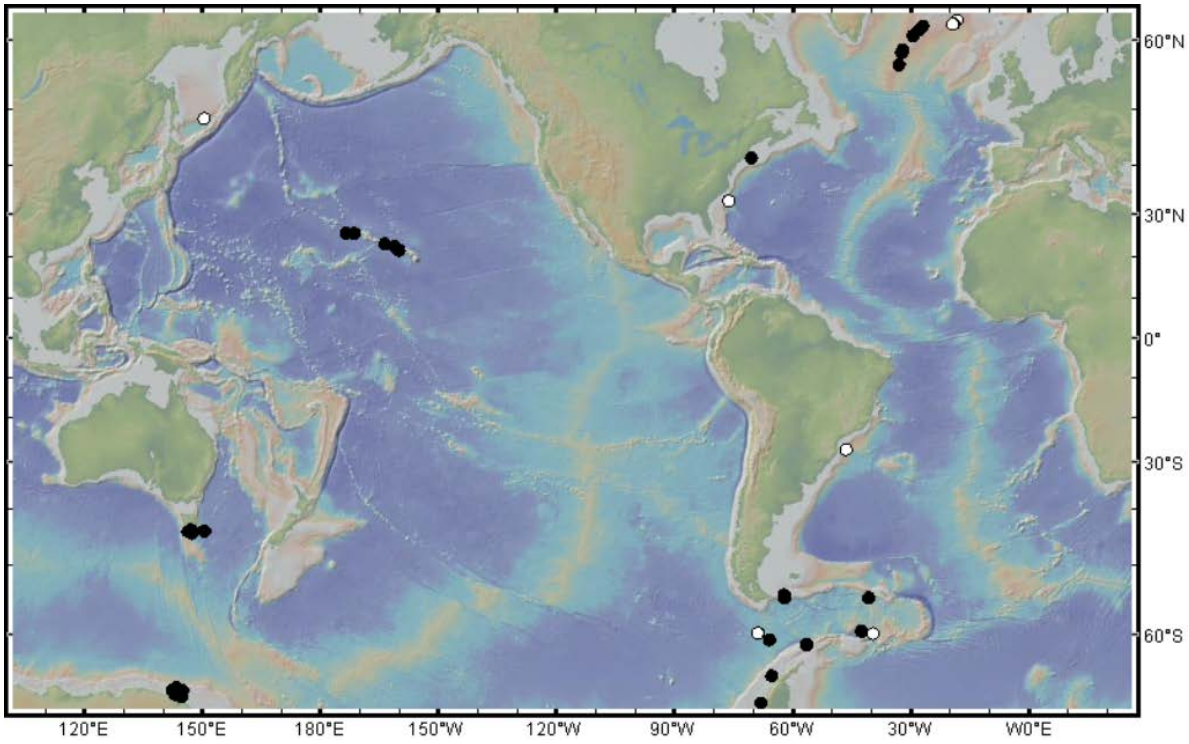


642

643

644 Figure 2: A) $\delta^{30}Si$ and B) $\Delta\delta^{30}Si$ for all sponges from different ocean basins. The
645 modern sponges (open symbols) were measured without Mg doping, with error bars
646 showing $2\sigma_{SD}$ (~±0.2 ‰ for $\delta^{30}Si$ and 0.4 ‰ for $\Delta\delta^{30}Si$). The core-top spicules (solid
647 symbols) were measured with Mg doping, with error bars showing $2\sigma_{SD}$ (~±0.1 ‰ for
648 $\delta^{30}Si$).

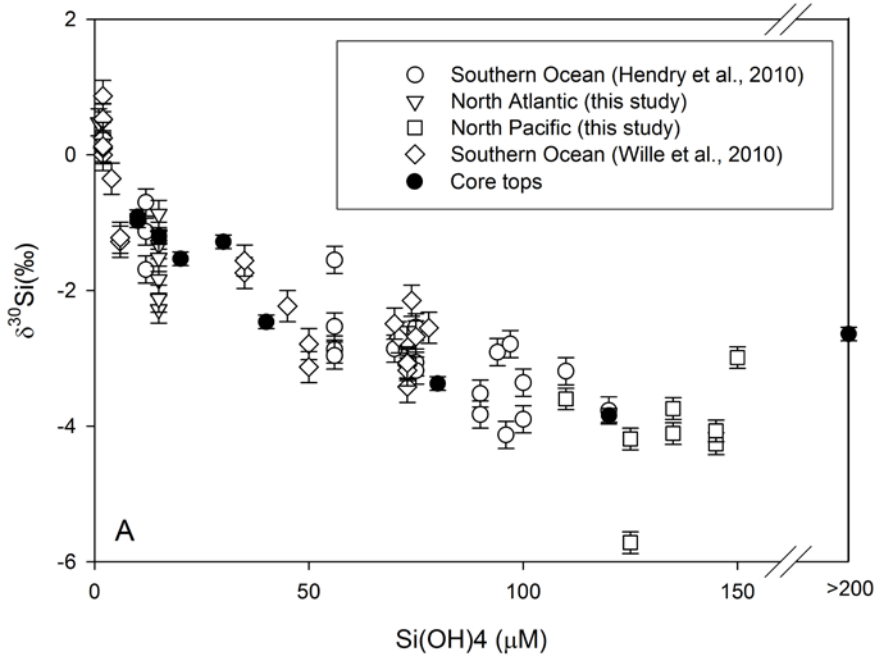


649

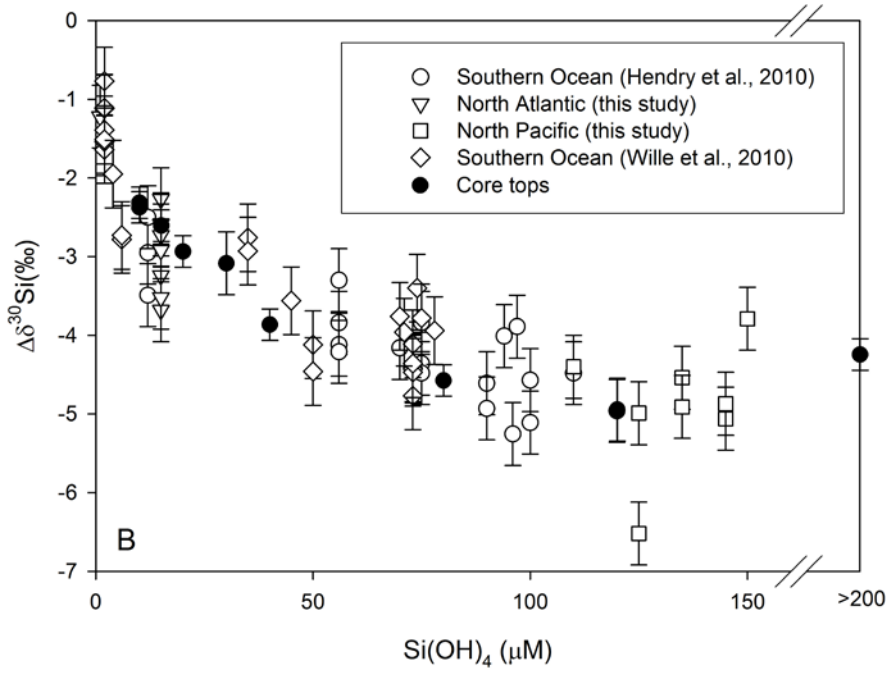


650

Figure 3: $\Delta\delta^{30}Si$ for all sponges from different ocean basins plotted against temperature (data from Hendry et al., 2010a; Wille et al., 2010; this study, www.ewoce.org, http://www.nodc.noaa.gov). Note that the larger number of samples from the Southern Ocean biases the relationship between apparent fractionation and temperature (grey symbols): the North Pacific and Atlantic data cover the same range of apparent fractionation values, but in a limited temperature window (black symbols). $2\sigma_{SD}$ on $\Delta\delta^{30}Si$ values ~ 0.4‰.

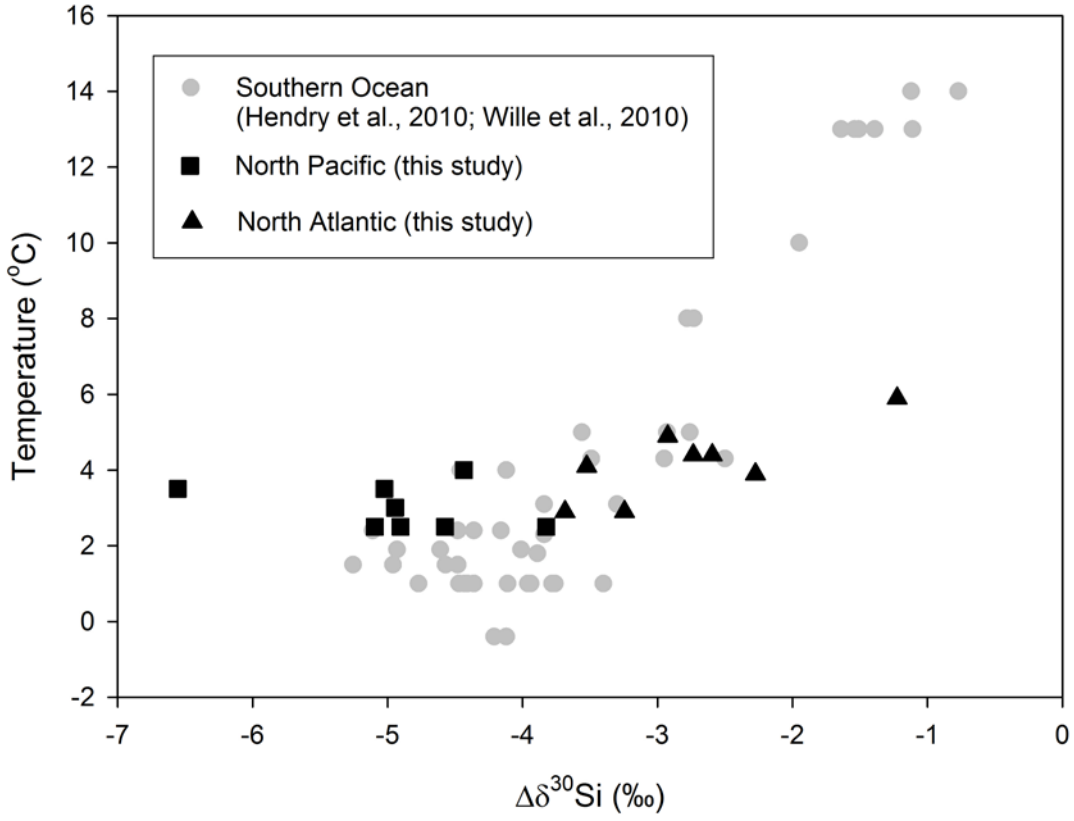

Figure 4: Fractionation of Si isotopes by sponges during uptake processes. A) A cartoon of the fractionation model used in this study. It should be noted that the model used here is a simplification of sponge silicification, and other models for silicification mechanisms exist (e.g. Müller et al., 2007; Maldonado & Riesgom 2007). Seawater enters the sponge via pores, lined with pinacocyte cells, and is taken up into the sclerocyte cells where silica formation is initiated. Silicification of large spicules occurs extracellularly in association with an organic matrix, and is controlled by protein interactions (Schröder et al., 2008). The fractionation parameters are described in the main text. B-C) The misfit between predicted $\varepsilon_f$ and observed $\Delta\delta^{30}Si$ for the whole dataset (the misfit function is defined as $(\varepsilon_f - \Delta\delta^{30}Si)^2$ shown by the solid line), and corresponding value of $\varepsilon_{tl}$ that results in the minimum misfit (circles), for different values of $\Delta\varepsilon_p$ substituted into Equations 4 and 5, using values from B) Reincke & Barthel, 1997 and C) Maldonado et al., 2011. The isotope data for sponges grown in low $Si(OH)_4$ conditions (<2 μM) show an average $\Delta\delta^{30}Si$ of -1.3 ± 0.3‰ ($\sigma_{SD}$), shown by the black arrows, which should equal the value of $\varepsilon_{tl}$.

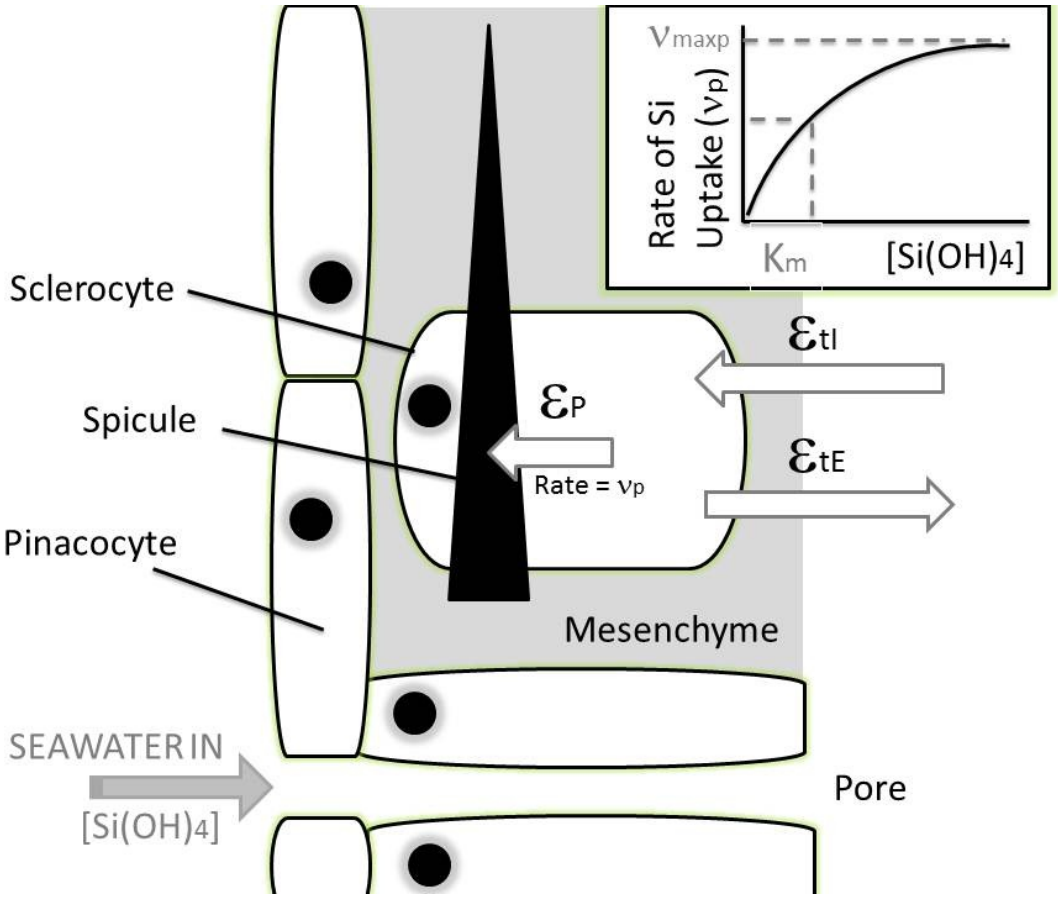

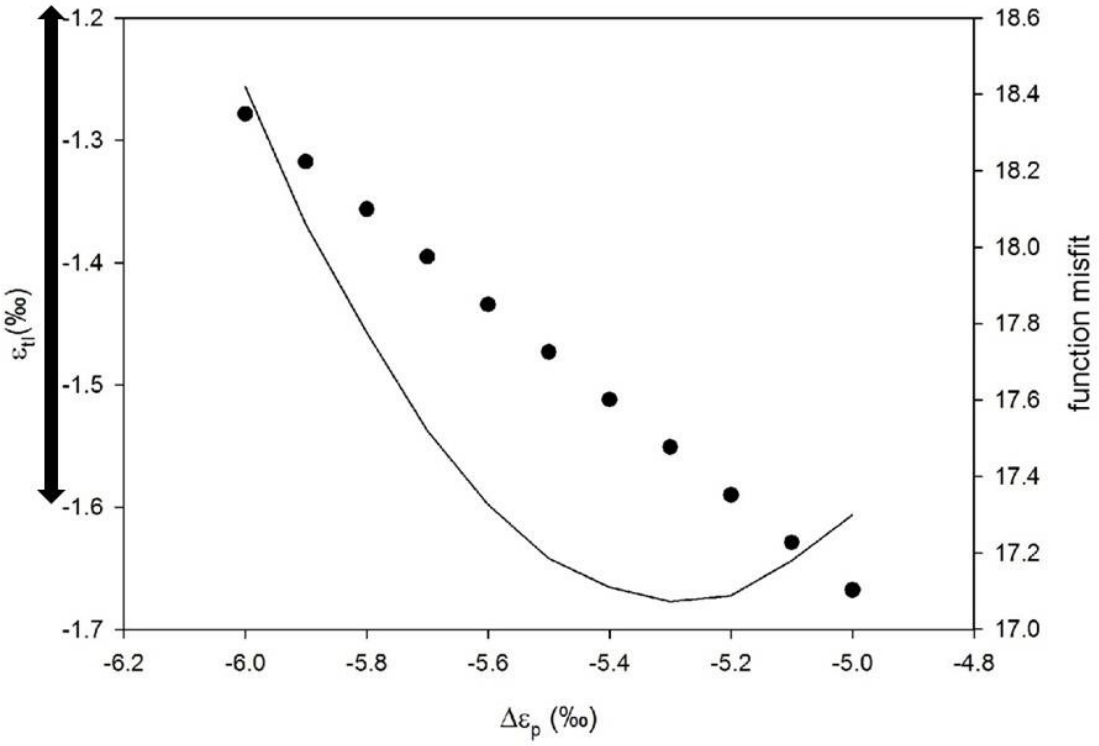
-1.2
-1.3
-1.4
-1.5
-1.6
-1.7
$\varepsilon_{tl}$(‰)
18.6
18.4
18.2
18.0
17.8
17.6
17.4
17.2
17.0
function misfit
-6.2
-6.0
-5.8
-5.6
-5.4
-5.2
-5.0
-4.8
$\Delta\varepsilon_p$ (‰)

676

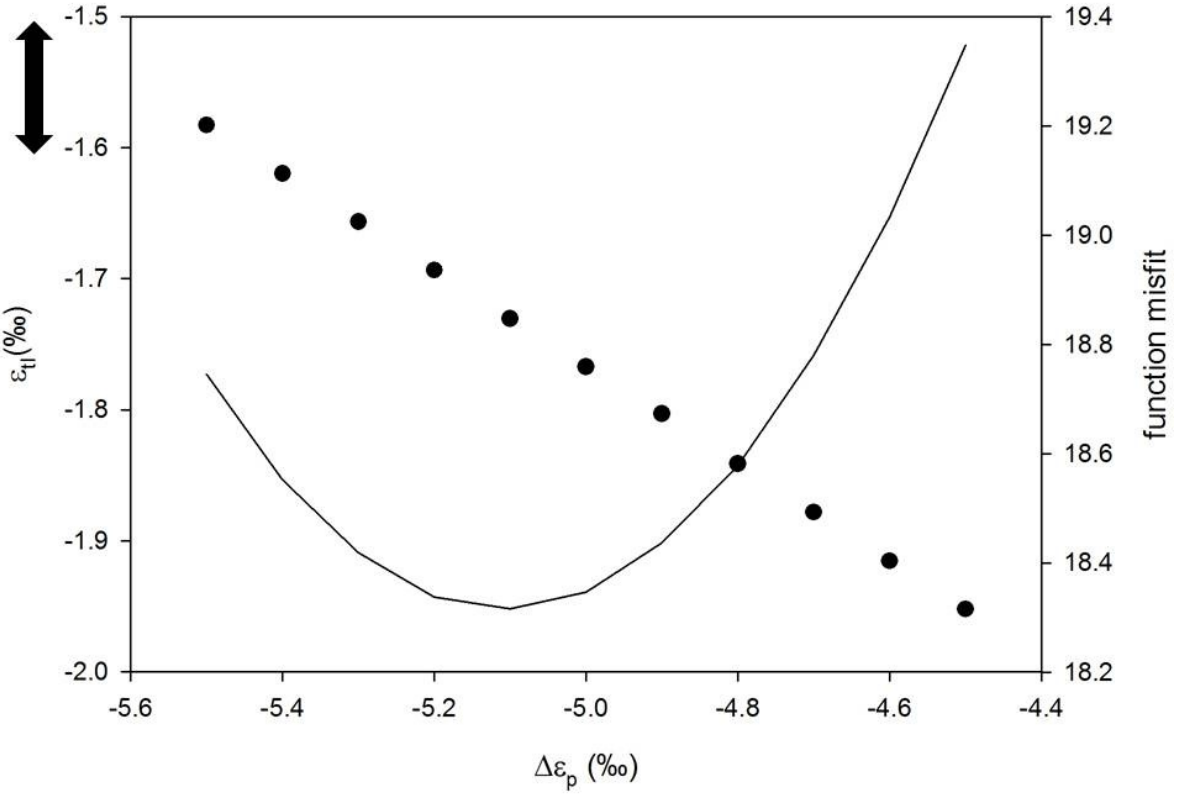
-1.5
-1.6
-1.7
-1.8
-1.9
-2.0
19.4
19.2
19.0
18.8
18.6
18.4
18.2
-5.6
-5.4
-5.2
-5.0
-4.8
-4.6
-4.4
$\varepsilon_{tl}$(‰)
function misfit
$\Delta\varepsilon_p$ (‰)

677

678

679 Figure 5: The observed $\Delta\delta^{30}Si$ vs. $\varepsilon_f$ predicted using the sponge silicon uptake model
680 for the uptake kinetics of Reincke & Barthel, 1997 and Maldonado et al., 2011 (shown
681 as inset). The solid lines show the 1:1 slope ± $2\sigma_{SD}$ uncertainty for the $\Delta\delta^{30}Si$ values.
682 Error bars show ±$2\sigma_{SD}$.

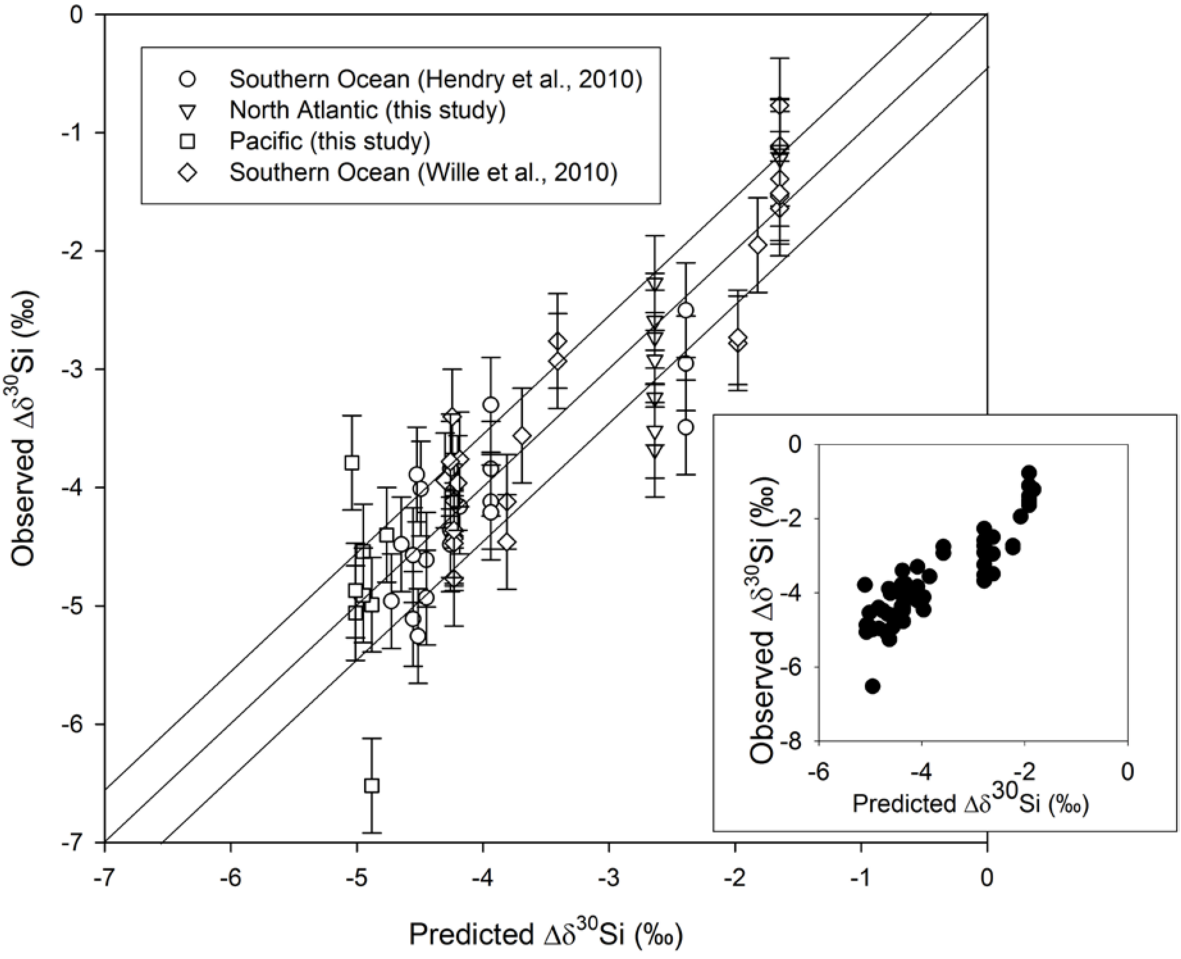


683

684

Figure 6: Field data showing the apparent change in diatom fractionation factor with ambient Si(OH)4 concentration. Data from Varela et al., 2004; Cardinal et al., 2005, Fripiat et al., 2009, and the core-top diatom value from Table 1 ($2\sigma_{SD}$ on $\Delta\delta^{30}Si$ values ~ 0.4‰). The grey bar shows the fractionation factor of -1.1‰ from de la Rocha et al., 1997, with the same uncertainty of ±0.4‰. The dashed lines show the 95% confidence level.

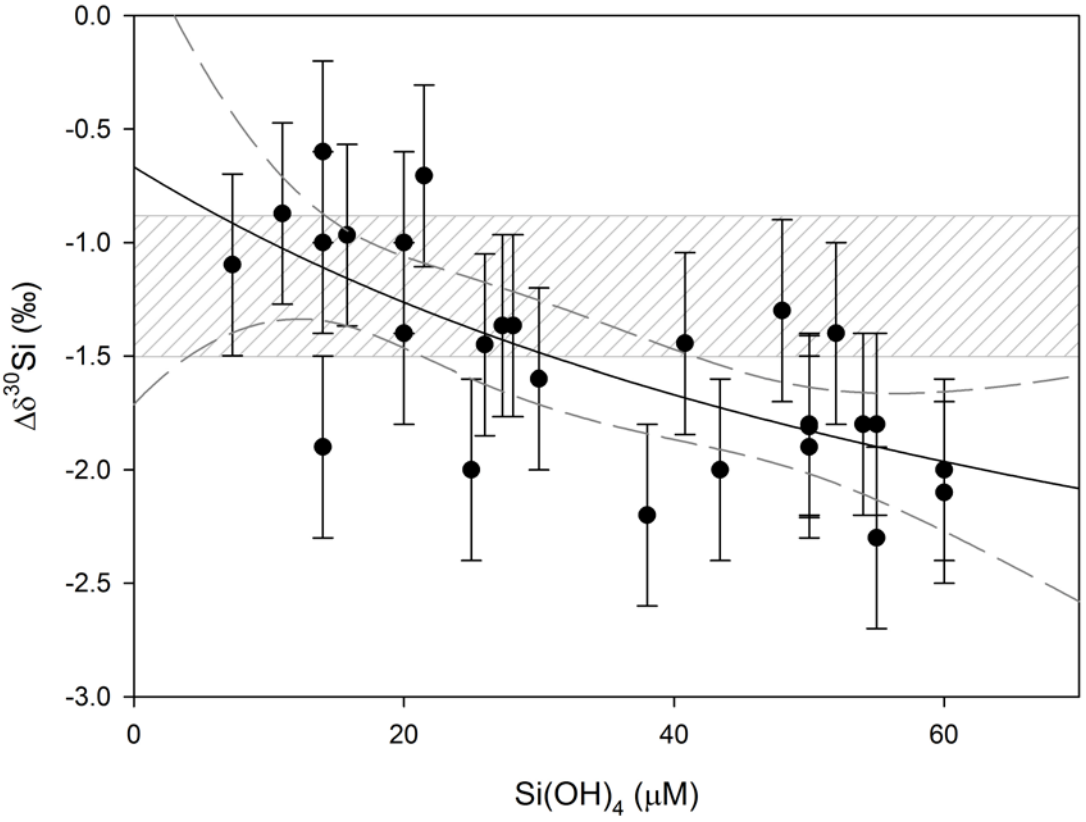

693 Figure 7: Core-top calibration of A) $\delta^{30}Si$ and B $\Delta\delta^{30}Si$ of sponges versus $Si(OH)_4$. The
694 solid line shows the predicted $Si(OH)_4$ using the regression analysis and the dashed
695 lines show the 95% confidence interval. The solid symbols show the samples used in
696 the regression analysis (<120 mM) and the open symbol shows the sample from the
697 Okhotsk Sea).

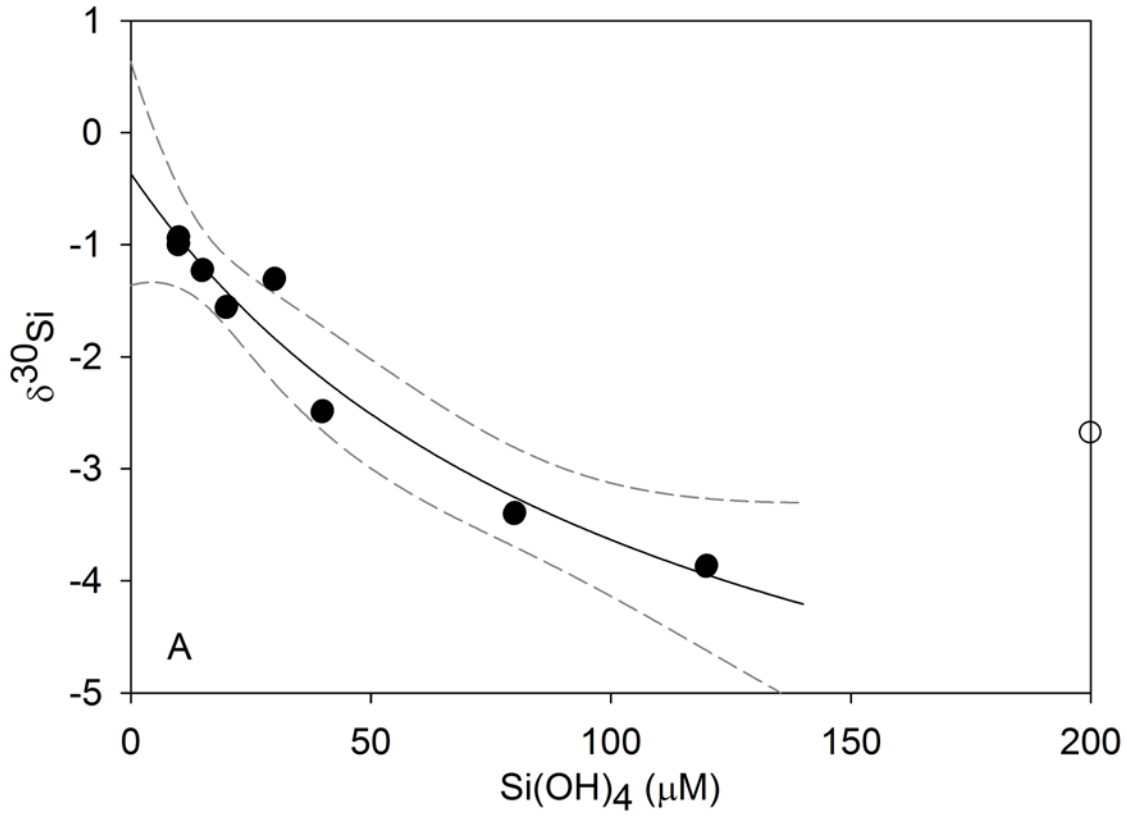
1
0
-1
-2
-3
-4
-5
$\delta^{30}Si$
A
0
50
100
150
200
$Si(OH)_4$ (μM)

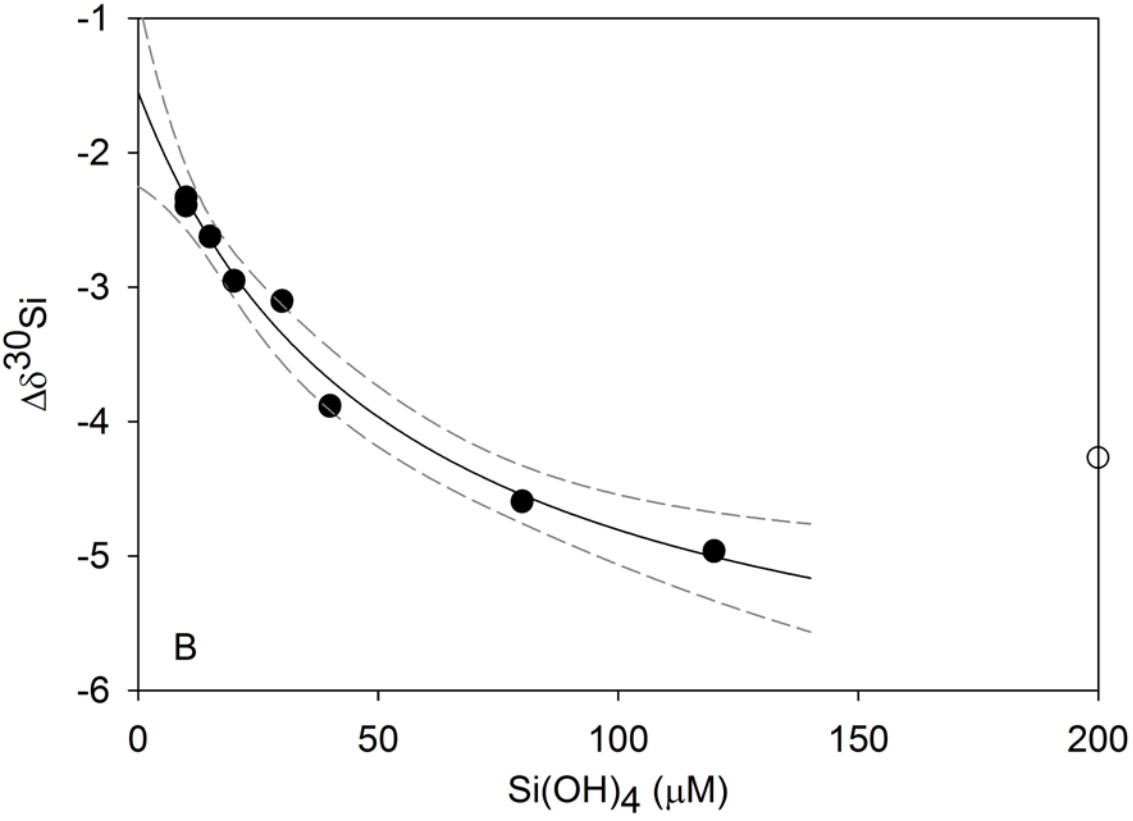
-1
-2
-3
-4
-5
-6
$\Delta\delta^{30}Si$
B
0
50
100
150
200
$Si(OH)_4$ (μM)

698

699

700

701

| Specimen | Species | Lat | Long | Depth (m) | $Si(OH)_4$ (μM) | $\delta^{29}Si$ (‰) | $\delta^{30}Si$ (‰) |
|---|---|---|---|---|---|---|---|
| *LMG08* [a] | Unknown | 64.78 S | 68.23 W | 600 | 105-110 | -1.75 (0.06) | -3.43 (0.15) |
| *LMG08* [b] | | | | | | -1.77 (0.04) | -3.44 (0.09) |
| *LMG08* [c] | | | | | | -1.72 (0.07) | -3.37 (0.17) |
| *LMG08* [d] | | | | | | | -3.33 |
| *N. Atlantic* | | | | | | | |
| D10[a] | Unknown | 56.88 N | 33.00 W | 2150 | 15 | -0.89 | -1.84 |
| D18[e] | Unknown | 58.51 N | 32.32 W | 1520 | 15 | -0.45 | -0.87 |
| D19A[e] | Unknown | 58.90 N | 31.98 W | 1720 | 15 | -1.12 | -2.28 |
| D26[a] | Unknown | 60.72 N | 29.45 W | 1250 | 15 | -1.00 | -2.12 |
| D29[a] | Unknown | 61.41 N | 27.86 W | 1105 | 15 | -0.61 | -1.19 |
| D30A[a] | Unknown | 61.57 N | 27.56 W | 1021 | 15 | -0.73 | -1.33 |
| D31A[a] | Unknown | 61.87 N | 27.01 W | 864 | 15 | -0.75 | -1.52 |
| Woods Hole[a] | Unknown | 41.53 N | 70.67 W | 10 | <1 | +0.21 | +0.48 |
| *Pacific* | | | | | | | |
| P4-299-10 [a] | Unknown | 22.72 N | 161.67 W | 1000 | 110 | -1.87 | -3.60 |
| 1097479[a] | *Caulophacus* sp. | 25.80 N | 173.43 W | 1798 | 145 | -2.05 | -4.07 |
| 1097480[a] | | 25.80 N | 173.43 W | 1802 | 145 | -2.19 | -4.27 |
| 1097533[a] | Hexactinellid *Farrea* sp. | 25.70 N | 171.45 W | 1810 | 150 | -1.52 -1.56 | -2.92 -3.06 |
| 1097536[a] | | 25.70 N | 171.45 W | 1488 | 135 | -2.12 | -4.11 |
| 1097539[a] | Hexactinellid *Farrea* sp. | 25.67 N | 171.41 W | 1206 | 125 | -2.99 | -5.72 |
| 1097541[a] | | 25.67 N | 171.41 W | 1206 | 125 | -2.13 | -4.19 |
| 1097570[a] | *Bathydorus* sp. *Trichasterina* sp. | 23.30 N | 163.68 W | 1443 | 135 | -1.91 | -3.74 |
| *Dredge sediments* | | | | | | | |

| | | | | | | | |
|---|---|---|---|---|---|---|---|
| Sars sea-mount NBP0805-DR34 [a] | | 59.73 S | 68.73 W | 850 | 80 | -1.77 | -3.39 |
| NBP1103-DH91 [a] | | 59.72 S | 68.87 W | 650 | 40 | -1.30 | -2.59 |
| NBP1103-DH91 [b] | | | | | | -1.29 | -2.48 |
| *Core-top spicules* | | | | | | | |
| Newmeyanov, 25, GGC15[a] | | 51.1 N | 168.1 W | 1980 | 200 | -1.32 | -2.66 |
| Newmeyanov, 25, GGC15[b] | | | | | | -1.26 | -2.53 |
| KNR-140-2-GGC56[a] | | 32.94 N | 76.30 W | 1400 | 15 | -0.66 | -1.27 |
| KNR-140-2-GGC56[b] | | | | | | -0.60 | -1.22 |
| ATII-94-1PC[b] | | 62 .58 N | 18.23 W | 1177 | 10 | -0.46 | -0.99 |
| ATII-94-9PG[a] | | 62.12 N | 19.04 W | 2090 | 20 | -0.83 | -1.61 |
| ATII-94-9PG[b] | | | | | | -0.72 | -1.55 |
| ATII-94-10PC[b] | | 62.15 N | 19.33 W | 1564 | 10 | -0.40 | -0.93 |
| GeoB2107[a] | | 27.18 S | 46.45 W | 1048 | 30 | -0.68 | -1.27 |
| PC034[e] | | 59.79 S | 39.60 W | 1652 | 120 | -1.96 | -3.86 |
| Diatom samples from Ryder Bay, Antarctica (core BC388) [e] | | 67.57 S | 68.23 W | 500 | 60 | -0.03 | -0.01 |

| | | | | | | | |
|---|---|---|---|---|---|---|---|
| | | | | | | | |

a =measured by Neptune MC-IC-MS (WHOI) without Mg doping (typically mean of triplicate measurements); b = measured by Neptune MC-IC-MS (WHOI) with Mg doping; c = mean value from 3 different laboratories from Hendry et al., 2010b; d = measured by M. Brzezinski and C. Beucher (UCSB) by IRMS, shown as the mean of two duplicates; e = measured by NuPlasma MC-ICP-MS (Oxford) without Mg doping (Hendry et al., 2010a). Numbers in parentheses show $2\sigma_{SD}$ long-term variability. Silicic acid concentrations are estimated from ewoce sections (www.ewoce.org) with an approximate error of 5μM, which has not been taken into consideration in the statistical analysis.

Table 1: Samples and silicon isotopic compositions of modern sponges and core-tops.

711 Table 2: Seawater $\delta^{30}Si(OH)_4$ values used in this study; [a] from de la Rocha et al. (2000);
712 [b] from Hendry et al. (2010a); [c] from Wille et al. (2010) adapted from Cardinal et al.
713 (2005); [d] from Beucher et al. (2008).

| Ocean basin/water mass | Depth (m) | $\delta^{30}Si(OH)_4$ (‰) |
|---|---|---|
| North Atlantic | 1000-2000 | +1.4[a] |
| North Pacific | 1000-2000 | +0.8[a] |
| Southern Ocean | | |
| AAIW | ~300 | +1.8[b] |
| CDW | 400-1000 | +1.3 to +1.4[b,c] |
| | 1000-2000 | +1.1[b,c] |
| Sub-surface (depleted $Si(OH)_4$) | 50-150 | +1.7 to +1.9 [a,c,d] |
| North Pacific (highly enriched in $Si(OH)_4$) | 2000-2500 | +1.6 to +1.7 [d] |
| Near surface in Ryder Bay, Antarctica | | +1.8[b] |

714

715